Mass Redistribution Causes the Structural Richness of Ion-Irradiated Surfaces

Charbel S. Madi, Eitan Anzenberg, Karl F. Ludwig, Jr., and Michael J. Aziz

Phys. Rev. Lett. **106**, 066101 — Published 8 February 2011

DOI: 10.1103/PhysRevLett.106.066101

Mass Redistribution Causes the Structural Richness of Ion-Irradiated Surfaces

Charbel S. Madi[1], Eitan Anzenberg[2], Karl F. Ludwig, Jr.[2], and Michael J. Aziz[1]

[1]*Harvard School of Engineering and Applied Sciences, Cambridge Massachusetts 02138, USA*

[2]*Department of Physics, Boston University, Boston Massachusetts 02215, USA*

(Submitted: 2 June 2010; Revised 16 September 2010)

We show that the "sputter patterning" topographical instability is determined by the effects of ion impact-induced prompt atomic redistribution and that sputter erosion - the consensus predominant cause - is essentially irrelevant. We use Grazing Incidence Small Angle X-Ray Scattering to measure *in situ* the damping of noise or its amplification into patterns via the linear dispersion relation. A model based on the effects of impact-induced redistribution of those atoms that are *not* sputtered away explains both the observed ultra-smoothening at low angles from normal ion incidence and the instability at higher angles.

PACS numbers: 68.49.Sf, 81.65.Cf, 81.16.Rf

Spontaneous self-organization processes have aroused intense interest due to their potential for transcending the constraints of lithography for device fabrication. Uniform ion irradiation of solid surfaces where the energy loss is dominated by nuclear collision cascades (typically 10^2-10^4 eV) often causes a self-organized topographic pattern of corrugations, holes or dots [1]. Since its discovery nearly half a century ago [2], it has been suspected that this "sputter pattern" formation is caused by sputter erosion effects. The ero-

sion-based paradigm was established firmly 22 years ago when the destabilizing effect of the surface curvature-dependent [3] sputter yield (atoms removed per incident ion) was incorporated into the linear stability theory of Bradley and Harper [4] (BH). In BH theory the characteristic length scale of the pattern originates from differing wavenumber dependences of two competing effects: the destabilizing effect of a sputter yield that increases with increasing concave curvature, and the stabilizing effect of capillarity-driven surface diffusion. Although BH theory explains several experimental observations, its prediction that an initially flat surface will display a pattern-forming instability at all incidence angles is contradicted by a number of experimental studies on amorphous surfaces such as quartz glass [5] and room-temperature amorphous sapphire [6] and silicon [7-9], for which there are no potentially confounding effects of singular crystallographic surface energetics and kinetics [10]. These studies report rippled surfaces at high angles θ of deviation from normal incidence, with a transition to a stable flat surface with decreasing θ. Several authors [7,11,12] have analyzed an impact-induced prompt mass redistribution effect as potentially a small modification of the BH model, sufficient to rescue stability at low angle and perhaps moderating the erosion-driven instability at high angle. We show here that, as far as the stability/instability transition is concerned, the redistribution effect is essentially the whole story – not only the cause of stability at low angle, but also the cause of instability at high angle – and that the erosive effect is essentially irrelevant.

A linear stability analysis of a flat, isotropic, monatomic surface undergoing ion beam erosion describes the evolution of a surface height profile $h(x,y,t)$ according to:

$$\frac{\partial h(x,y,t)}{\partial t} = S_X(\theta)\frac{\partial^2 h}{\partial x^2} + S_Y(\theta)\frac{\partial^2 h}{\partial y^2} - B\nabla^4 h + \zeta(x,y,t) \qquad (1)$$

where h is measured in the frame of reference fixed on the average surface height, $S_X(\theta)$ and $S_Y(\theta)$ are the curvature coefficients causing surface instability (stability) when negative (positive), and B is a material parameter describing relaxation and containing the surface free energy and either the surface diffusivity [4] or the viscosity of the ion-stimulated layer [13]. $\zeta(x,y,t)$ is a Gaussian white noise [14]. In this work, we take care to identify and confine our experimental study to the linear regime of exponential amplification at early time and low fluence for which this analysis is valid. Fourier methods permit a straightforward solution: $h(x,y,t)$ is written as the sum of normal modes $\propto e^{\omega(\mathbf{q})t}e^{i\left(q_x x + q_y y\right)}$ of wave vector $\mathbf{q}$ which, when inserted into Eq. (1), determine the amplification rate $R(\mathbf{q})$:

$$R(\mathbf{q}) \equiv \mathrm{Re}(\omega(\mathbf{q})) = -S_x q_x^2 - S_y q_y^2 - B\left(q_x^2 + q_y^2\right)^2 . \tag{2}$$

The stability of a flat surface is determined by the sign of the maximum growth rate $\max\{R(\mathbf{q})\}$; $\max\{R(\mathbf{q})\} < 0$ corresponds to stability.

The evolution of an arbitrary surface can be understood in terms of its spatial frequency spectrum $h(\mathbf{q},t) = \iint h(x,y,t)\exp^{-i\left(q_x x + q_y y\right)} dxdy$, where $h(\mathbf{q},t)$ is the spectrum of spatial frequencies in the surface structure. Combining the roughening and smoothing processes leads to the following linear equation governing the behavior of $h(\mathbf{q},t)$ through a spatial Fourier transform of Eq. (1):

$$\frac{d\left|h(\mathbf{q},t)\right|^2}{dt} = 2\,\mathrm{R}(\mathbf{q})\left|h(\mathbf{q},t)\right|^2 + \alpha , \tag{3}$$

where $|h(\mathbf{q},t)|^2$ is the structure factor of the surface profile and α is the structure factor of the stochastic white noise $\zeta(x,y,t)$. Integrating this equation yields the time-dependent behavior of the structure factor:

$$\left|h(\mathbf{q},t)\right|^2 = \exp\left(2R(\mathbf{q})\ t\right)\left(\left|h(\mathbf{q},0)\right|^2 + \frac{\alpha}{2R(\mathbf{q})}\right) - \frac{\alpha}{2R(\mathbf{q})}, \qquad (4)$$

where $h(\mathbf{q},0)$ is the initial roughness spectrum. The real-time diffuse scattering intensity in a Grazing Incidence Small Angle X-ray Scattering (GISAXS) geometry is directly proportional to the structure factor $|h(\mathbf{q},t)|^2$ and its measurement allows us, through Eq. (4), to directly determine in real time the linear dispersion relation $R(\mathbf{q})$ as well as the magnitude of the noise term α. From Eq. (4), we see that where $R(\mathbf{q})$ is positive, the amplitude of that Fourier mode will increase exponentially in time and fluence, and where $R(\mathbf{q})$ is negative, the amplitude will asymptotically approach a steady-state value of $\alpha /(-2R(\mathbf{q}))$.

We used GISAXS to measure in real time the linear dispersion relation characterizing the damping or amplification of small perturbations with wavenumber q_x ranging over about an order of magnitude in "parallel mode": wave vector parallel to the projection of the ion beam on the surface of average orientation. Real time monitoring of 1 keV Ar^+ ion bombarded Si(001) (*p* type, 1-10 Ω cm) surface evolution at room temperature is performed in a custom-built X-ray ultrahigh vacuum chamber (base pressure 1×10^{-9} Torr) at the National Synchrotron Light Source X-ray beamline X21. A photon wavelength of 0.124 nm is selected by a Si(111) monchromator passing about 10^{12} photons/s. In the GISAXS geometry, we take the *z*-direction to be along the sample normal, the *y*-direction to be along the projected direction of the X-ray beam onto the sample surface, and the *x*-direction, the coordinate along which the linear position sensitive detector is oriented, to be along the sample surface and parallel to the projection of the ion beam [15]. The argon ions were generated using a PHI ion gun from Physical Electronics, Inc. The beam di-

ameter was approximately 1.5 cm and the flux in the experiments was 2×10^{12} ions/(cm^2 s) reckoned in a plane perpendicular to the ion beam.

GISAXS real-time measurements of the roughening and smoothing processes are displayed in Fig. 1 and Fig. 2. Fig. 1(a) shows real-time roughening of an initially smooth amorphous Si substrate during bombardment at $\theta = 65°$ from normal at various collection time intervals. The increase in the satellite peak intensity at $q_x \approx 0.25$ nm^{-1} corresponds to parallel mode ripples with a characteristic wavelength $\lambda \approx 25$ nm, as corroborated by Atomic Force Microscopy (AFM) images [14]. Fig. 1(b) displays the corresponding color map intensity plot of the roughening process during bombardment at $\theta = 65°$ from normal. Fig. 1(c) illustrates exponential amplification of the surface fluctuations, indicating a positive value of the amplification rate $R(q_x$=0.278 nm$^{-1})$ at $\theta = 65°$. At higher wavenumber (q_x=0.482 nm^{-1}) at this same θ, amplification of the diffusely scattering intensity by the noise source α with damping by a negative value of R is illustrated in Fig. 1(d). Thus a sufficient time span of the real-time GISAXS measurement permits us to distinguish between a noise-enhanced scattering that is nevertheless damped by a negative value of $R(q_x)$, and amplification by a positive value of $R(q_x)$. Fig. 2(a) shows a real-time GISAXS series of the smoothening process of an initial rippled sample obtained at $\theta = 65°$ and fluence of 1.8×10^{16} ions/cm^2 and subjecting it to normal incidence ion bombardment with a data collection time interval of 10 s. Note that the satellite peak intensity decreases upon irradiation which indicates that the rippled surface is being smoothed, enabling us to directly determine the smoothening coefficient $R(q_x)$. Fig. 2(b) shows the smoothening of the scattering intensity by a negative value of R at mode $q_x = 0.278$ nm^{-1} for normal incidence ion bombardment.

For each Fourier mode q_x in Fig. 1(a) and 2(a), we fit the evolution of the structure factor to Eq. (4) with two adjustable parameters: the amplification rate $R(q_x)$ and the noise source structure factor $\alpha(q_x)$. For this 2-dimensional surface of chi-square vs. R and α, we find the optimum R and α values that minimize chi-square along the surface. Fig. 3 displays the calculated amplification rates $R(q_x)$ thus obtained and their corresponding uncertainties at the 90% confidence level. Unique behavior is apparent at $\theta = 45°$, where there is no clear sign of damping or amplification in the evolution of the structure factor and the error bars in Fig. 3 are large and straddle the axis. Because this angle is in the immediate vicinity of the previously-determined [8,9] phase transition point -- where the quadratic term vanishes -- the interaction between noise and nonlinear effects, which these experiments were designed to minimize, may provide an unavoidable contribution to the measured behavior. Hence we exclude the data at 45° from the analysis described below.

The solid lines shown in Fig. 3 are generated by simultaneously fitting to Eq. (2) the set of the measured linear dispersion relations $R(q_x)$ at $\theta = 0°$, 20°, 30°, 35°, 50°, and 65°. Error bar weighted least-squares fitting is performed by allowing the quadratic coefficient S_X to vary independently for each incidence angle and the quartic coefficient B to vary as an angle-independent constant. $R(q_x)$ is fit well by the quadratic plus quartic functional form (Eq. (2)) for this energy and temperature. This functional form of the dispersion relation leads to a diverging-wavelength transition from patterns to flatness, or "bifurcation" [8]. The agreement between the experimentally determined critical angle $\theta_C \approx 47.5° \pm 2.5°$ of the transition from a parallel-mode instability to flat surfaces with decreasing θ and the value previously reported for the same ion and energy but using a dif-

ferent ion gun, vacuum chamber and sample holder [9] is remarkably good. As anticipated in the discussion above, the experimental dispersion relation for $\theta = 45°$ cannot be reproduced by the fit (dashed line in Fig. 3) to the data at the other angles.

The curvature coefficient $S_X(\theta)$ is decomposed into an ion-stimulated erosive component, $S_X^{\text{eros.}}(\theta)$, which is evaluated using the BH erosive model, and an ion-stimulated mass redistribution component, $S_X^{\text{redist.}}(\theta)$, modeled using the Carter-Vishnyakov (CV) model for impact-induced mass redistribution [7,11,16]. We modify both of these models by the empirical Yamamura correction factor [17] (see text §1 of [14]), which was developed to fit the sputter yield vs. incidence angle for a large variety of projectiles and targets, and rationalized as accounting for the increasingly incomplete development of the collision cascade as grazing incidence is approached, due to the absence of the solid above the surface. When we applied this empirical correction factor to the BH and CV models we did not modify the Yamamura correction in any way, so it brings with it no additional free parameters. The only free parameter in our analysis is one from the CV model: the absolute magnitude δ of the sum of the vector displacements of all recoiled atoms, per incident argon ion; treated as an adjustable parameter to optimize the fit of $S_X^{\text{eros.}}(\theta) + S_X^{\text{redist.}}(\theta)$ to the measured $S_X(\theta)$, we obtain a best fit value of $\delta = 65 \pm 5$ nm. This numerical value of δ for 1000 eV impacts is reasonable when compared to recent Molecular Dynamics (MD) simulations yielding $\delta \sim 10$ nm for 250 eV impacts, as is the parameter-free $S_X^{\text{eros.}}(\theta)$ [18].

The curvature coefficient leading to destabilization of the parallel mode ripples, $S_X(\theta)$, extracted from a fit of the x component of Eq. (2) to the data in Fig. 3, is

plotted in Fig. 4. The Bradley-Harper prediction for the erosive contribution ($S_X^{\text{eros.}}(\theta)$) is not only of the wrong sign but also is of such a small magnitude as to be irrelevant, except possibly at the most grazing angles of incidence where both erosion and redistribution effects converge to zero. The ion-stimulated mass redistribution effect $S_X^{\text{redist.}}(\theta)$, represented by the green curve in Fig. 4, dominates the erosive contribution $S_X^{\text{eros.}}(\theta)$ and is essentially the only considerable mechanism for determining smoothening and patterning under uniform ion beam irradiation. This result provides the first experimental confirmation of the conjecture [11,19] that the stability of irradiated surfaces could be dominated by impact-induced mass redistribution rather than erosion. A theoretical upscaling of MD simulations with no fitting parameters leads to the same conclusions [18].

The value of B obtained by fitting Eq. (2) to the measured dispersion relations $R(q_x)$ is consistent with that expected from ion-enhanced viscous flow in a thin surface layer experiencing radiation-enhanced fluidity. We obtain a theoretical value of B for this mechanism of 0.062 nm^4/s [14], which is in reasonable agreement with our best-fit experimental value of B = 0.011 nm^4/s.

In conclusion, the quadratic coefficient $S_X(\theta)$ that determines linear stability or instability has two contributions. The contribution from sputter erosion is essentially irrelevant – it is of the wrong sign to explain the experiments and is an order of magnitude too small. Impact-induced redistribution is the determining factor under the experimental conditions reported here, causing the observed stability at low angles and driving its own instability at high angles. Our synthesis of the BH and CV models and the empirical Yamamura correction factor accounts for the experimental results quite well with the sole adjustable parameter being δ, the magnitude of the summed displacements of the recoiled atoms. The

conclusion that erosion is essentially irrelevant for instabilities does not depend on the inclusion or exclusion of the empirical Yamamura factor. That the contribution of prompt redistribution effects to $S_X(\theta)$ entirely overwhelms that of erosion in both the stabilizing and destabilizing regimes is of profound significance, as it overturns the erosion-based paradigm that has dominated the pattern formation field for over two decades. Although it is conceivable that erosion effects might become non-negligible at higher ion energies or angles, or for crystalline materials where anisotropy can influence all the potentially relevant processes [1], it remains to be shown that erosion effects are actually important for stability or pattern formation in any physical experiment to date.

We thank S. A. Norris and M, P. Brenner for helpful discussions and L. Colakerol for technical assistance. C.S.M and M.J.A were supported by DE-FG02-06ER46335 and E.A. and K.F.L by NSF DMR-1006538. Use of the National Synchrotron Light Source, Brookhaven National Laboratory, was supported under Contract No. DE-AC02-98CH10886.

References

[1] W.L. Chan and E. Chason, J. Appl. Phys. **101**, 121301 (2007).

[2] M. Navez, D. Chaperot, and C. Sella, Comptes Rendus Hebdomadaires Des Seances De L Academie Des Sciences **254**, 240 (1962).

[3] P. Sigmund, J. Mater. Sci. **8**, 1545 (1973).

[4] R.M. Bradley and J.M. Harper, J. Vac. Sci. Technol. A **6**, 2390 (1988).

[5] F. Frost, R. Fechner, B. Ziberi, J. Vollner, D. Flamm, and A. Schindler, Journal of Physics-Condensed Matter **21**, 224026 (2009).

[6] H. Zhou, Y. Wang, L. Zhou, R.L. Headrick, A.S. Ozcan, Y. Wang, G. Ozaydin, and K.F. Ludwig, Phys. Rev. B **75**, 155416 (2007).

[7] G. Carter and V. Vishnyakov, Phys. Rev. B **54**, 17647 (1996).

[8] C.S. Madi, B. Davidovitch, H.B. George, S.A. Norris, M.P. Brenner, and M.J. Aziz, Physical Review Letters **101**, 246102 (2008).

[9] C.S. Madi, H.B. George, and M.J. Aziz, Journal of Physics-Condensed Matter **21**, 224010 (2009).

[10] Exceptions to the BH paradigm are recognized on single crystal metal surfaces of singular orientations [1], where gradual surface diffusion is destabilizing by the mechanism of J. Villain, J. De Physique I **1**, 19 (1991).

[11] B. Davidovitch, M.J. Aziz, and M.P. Brenner, Phys. Rev. B **76**, 205420 (2007).

[12] H. Zhou, L. Zhou, G. Ozaydin, K.F. Ludwig, and R.L. Headrick, Physical Review B **78**, 165404 (2008); G. Ozaydin, K.F. Ludwig, H. Zhou, L. Zhou, and R.L. Headrick, Journal of Applied Physics **103**, 033512 (2008).

[13] C.C. Umbach, R.L. Headrick, and K.C. Chang, Physical Review Letters **87**, 246104 (2001).

[14] See supplementary material at {URL will be inserted by AIP} for determination of values of coefficients and corroboration of GISAXS topography interpretation with AFM.

[15] G. Ozaydin, K.F. Ludwig, H. Zhou, and R.L. Headrick, J. Vac. Sci. Technol. B **26**, 551 (2008).

[16] M. Moseler, P. Gumbsch, C. Casiraghi, A.C. Ferrari, and J. Robertson, Science **309**, 1545 (2005).

[17] Y. Yamamura, Y. Itikawa, and N. Itoh, Report No. IPPJ-AM-26, 1983; Y. Yamamura, C. Mössner, and H. Oechsner, Radiat. Eff. **103**, 25 (1987); W. Eckstein, "Sputtering Yields," in *Sputtering by Particle Bombardment: Experiments and Computer Calculations from Threshold to MeV Energies*, edited by R. Behrisch and W. Eckstein (Springer, Berlin, 2007).

[18] S.A. Norris, J. Samela, C.S. Madi, K. Nordlund, M.P. Brenner, and M.J. Aziz, submitted.

[19] M.J. Aziz, Mat. Fys. Medd. Dan. Vid. Selsk. **52**, 187 (2006); N. Kalyanasundaram, M. Ghazisaeidi, J.B. Freund, and H.T. Johnson, Appl. Phys. Lett. **92**, 131909 (2008).

Figure Captions

FIG. 1 (color online). GISAXS *in situ* measurements of roughening during Ar^+ ion irradiation at 1000 eV energy with a flux of 2×10^{12} ions/(cm^2s), at room temperature and at θ = 65° from normal incidence. (a) Scattering intensity increasing with time over a 2-hour period; individual traces are not separated by constant time interval. Arrows indicate q_x-values of subsequent two panels. (b) Color map intensity plot of the roughening process during bombardment at θ = 65° from normal. (c) Exponential amplification by a positive value of the amplification rate $R(q_x = 0.278\ nm^{-1})$. (d) An increase in the diffuse scattering intensity by the noise source α with exponential damping by negative value of the amplification rate $R(q_x = 0.482\ nm^{-1})$ at θ = 65°.

FIG. 2 (color online). Time-resolved GISAXS at normal incidence ion beam smoothening. (a) Sample with initial topography of saturated ripples obtained at θ = 65° is ion beam smoothed at normal incidence. (b)Exponential decay by a negative value of the amplification rate $R(q_x = 0.278\ nm^{-1})$.

FIG. 3 (color online). Measured linear dispersion relation $R(q_x)$ obtained from Eq. (4) for several ion beam incidence angles. The curves represent the quadratic plus quartic functional form of Eq. (2), all with the same value of the quartic coefficient, B = 0.011 nm^4/sec, and independently varying the quadratic coefficient S_X for each incidence angle. The best-fit value of B was obtained while excluding from the fit the data obtained at θ = 45°. The blue dashed line represents the theoretical dispersion relation at θ = 45° ob-

tained by constraining the quartic coefficient B to 0.011 nm^4/s and allowing the quadratic coefficient $S_X(45^o)$ to vary freely. The inset represents a magnification of the 65° and 0° linear dispersion relations, showing a window of unstable Fourier modes at 65° and stability at all Fourier modes at 0°.

FIG. 4 (color online). Dependence of the best-fit quadratic coefficient $S_X(\theta)$ and theoretical curves $S_X(\theta) = S_X^{\text{eros.}}(\theta) + S_X^{\text{redist.}}(\theta)$ on deviation from normal ion incidence. $S_X^{\text{eros.}}(\theta)$ is from BH theory modified by the Yamamura correction function with no free parameters. $S_X^{\text{redist.}}(\theta)$ is our implementation of the Yamamura correction on the CV redistributive model with a single free parameter as discussed in the text.

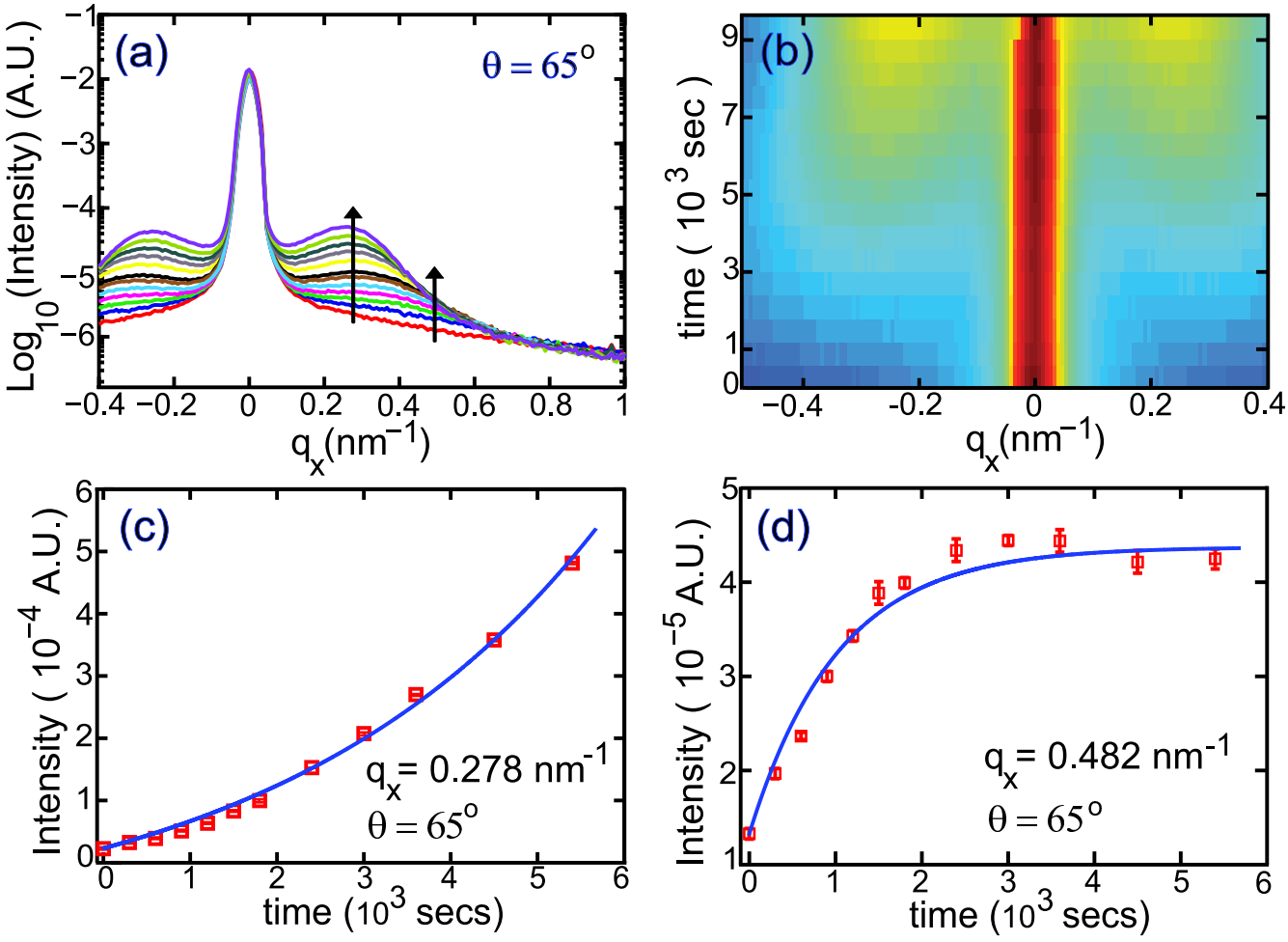

Figure 1 LT12076 28SEP2010

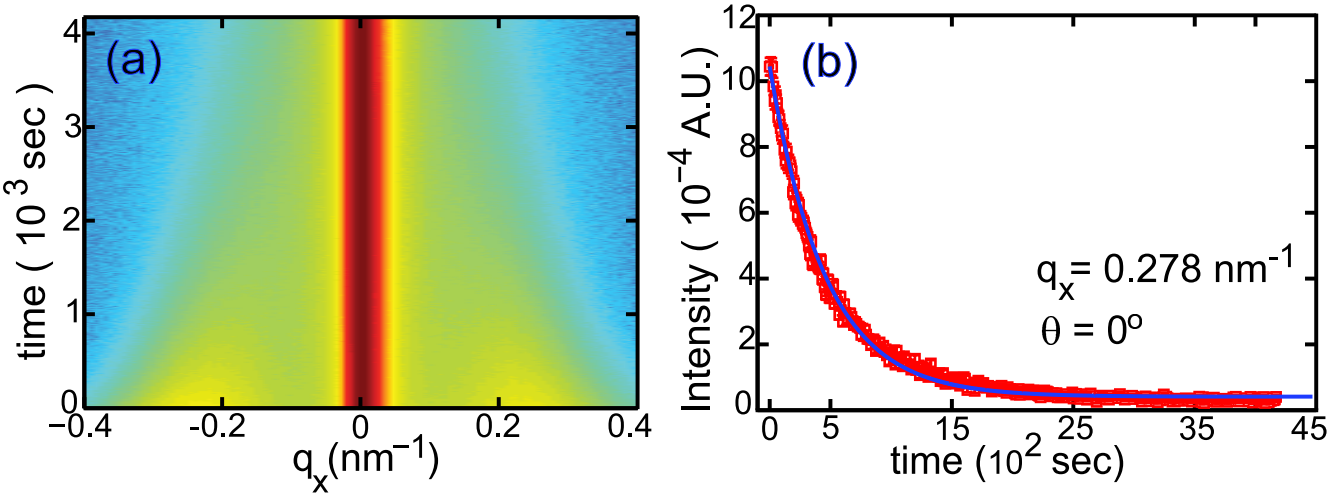

Figure 2 LT12076 28SEP2010

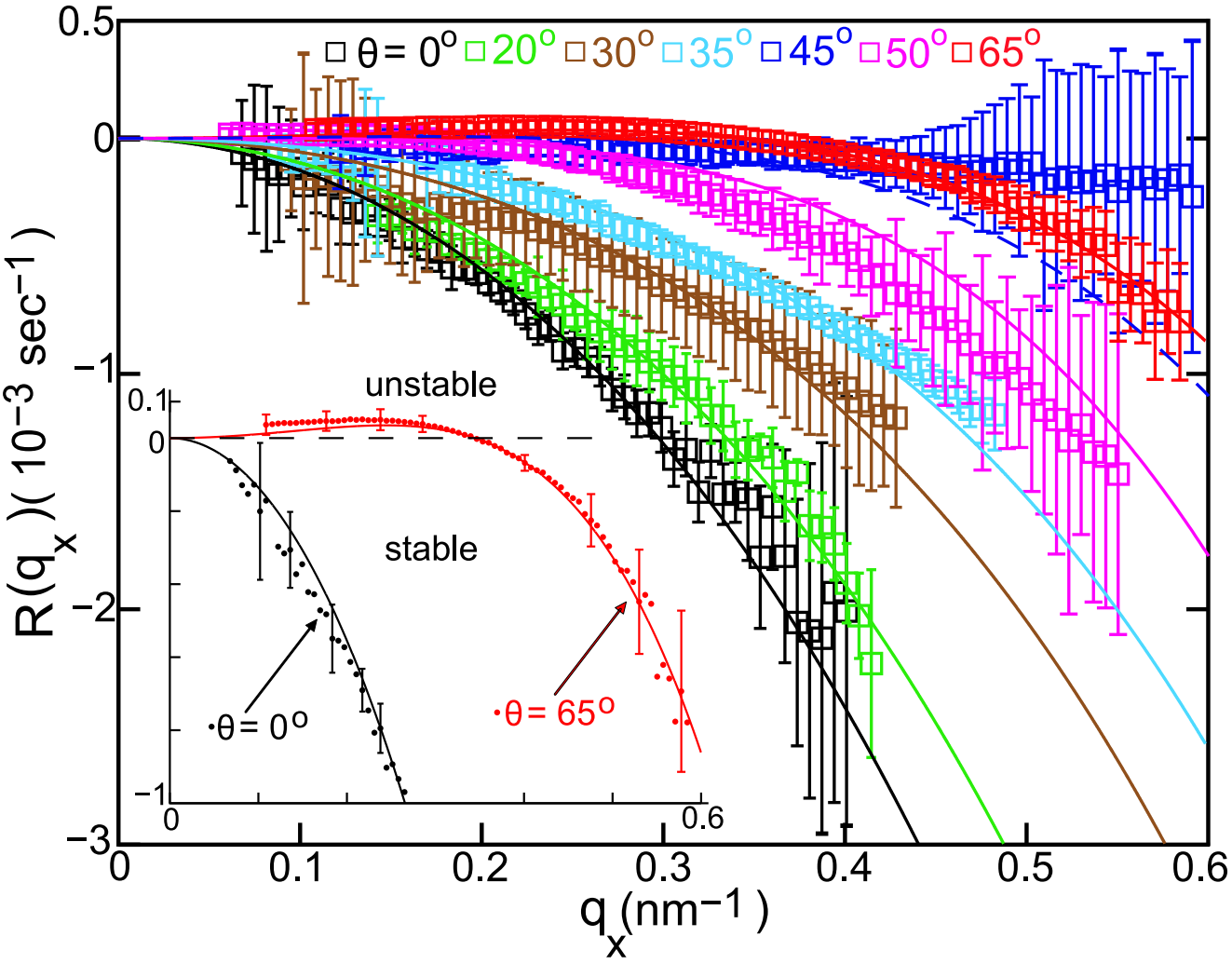

Figure 3 LT12076 28SEP2010

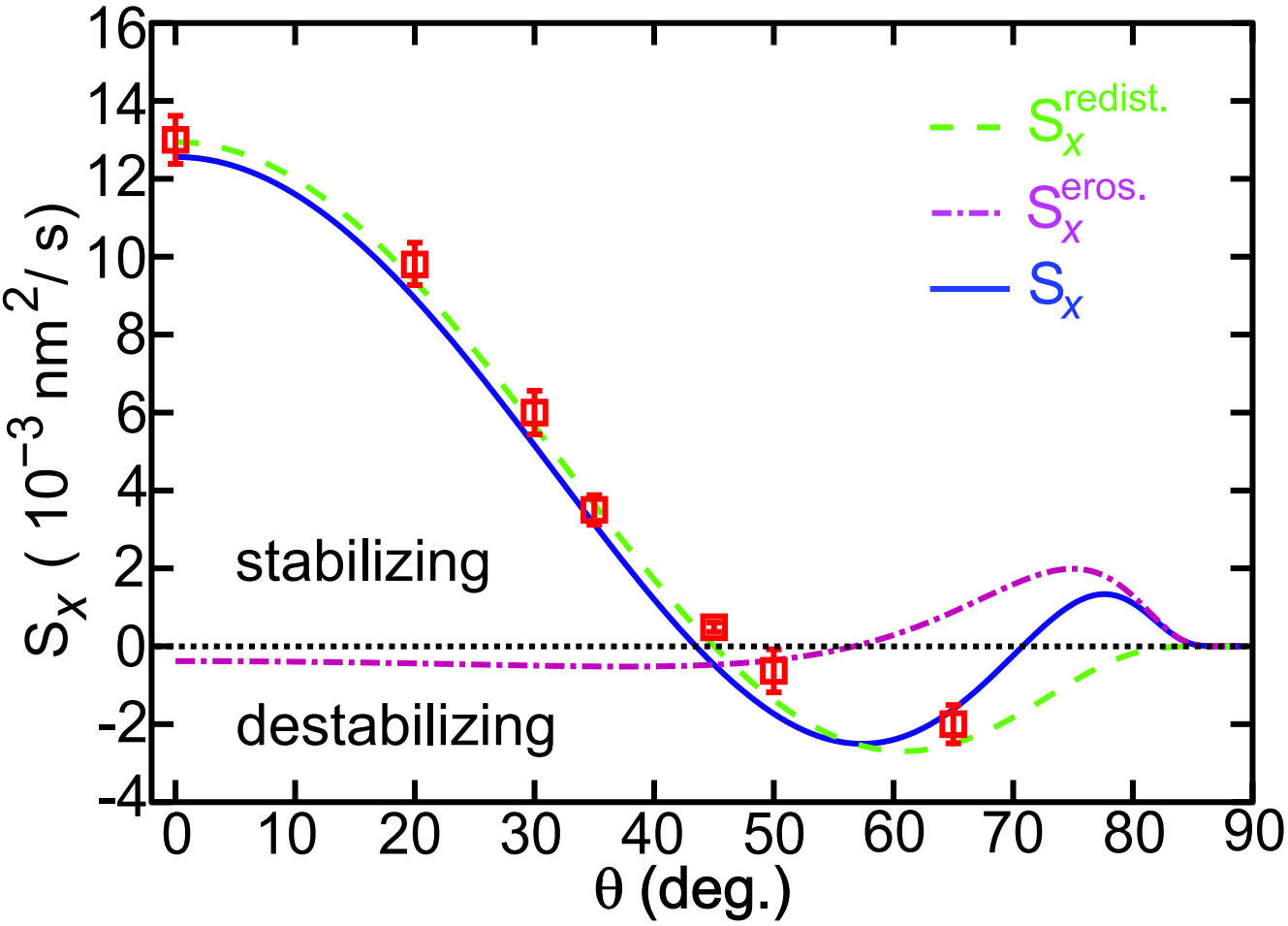

Figure 4 LT12076 28SEP2010